Atmos. Chem. Phys. Discuss., 13, 19193–19235, 2013
www.atmos-chem-phys-discuss.net/13/19193/2013/
doi:10.5194/acpd-13-19193-2013

Atmospheric Chemistry and Physics Discussions

Contribution of ammonium nitrate to aerosol optical depth and direct radiative forcing by aerosols over East Asia

R. S. Park, S. J. Lee, S.-K. Shin, and C. H. Song

School of Environmental Science and Engineering, Gwangju Institute of Science and Technology (GIST), Gwangju, 500-712, Korea

Received: 7 June 2013 – Accepted: 11 July 2013 – Published: 20 July 2013

Correspondence to: C. H. Song (chsong@gist.ac.kr)

Published by Copernicus Publications on behalf of the European Geosciences Union.

Abstract

This study focused on the contribution of ammonium nitrate (NH_4NO_3) to aerosol optical depth (AOD) and direct radiative forcing (DRF) by aerosols over an East Asian domain. In order to evaluate the contribution, CTM-estimated AOD was combined with satellite-retrieved AOD, utilizing a data assimilation technique, over East Asia for the entire year of 2006. Using the assimilated AOD and CTM-estimated aerosol optical properties, the DRF by aerosols was estimated over East Asia via a radiative transfer model (RTM). Both assimilated AOD and estimated DRF values showed relatively good agreements with AOD and DRF by aerosols from AERONET. Based on these results, the contributions of NH_4NO_3 to AOD and DRF by aerosols (Φ_{AOD} and Φ_{DRF}) were estimated for four seasons of 2006 over East Asia. Both Φ_{AOD} and Φ_{DRF} showed seasonal variations over East Asia within the ranges between 4.7 % (summer) and 31.3 % (winter) and between 4.7 % (summer) and 30.7 % (winter), respectively, under clear-sky conditions, showing annual average contributions of 15.6 % and 15.3 %. Under all-sky conditions, Φ_{DRF} varied between 3.6 % (summer) and 24.5 % (winter), showing annual average contribution of 12.1 % over East Asia. These annual average contributions of NH_4NO_3 to AOD and DRF are almost comparable to the annual average mass fractions of NH_4NO_3 to $PM_{2.5}$ and PM_{10} (17.0 % and 14.0 %, respectively). Φ_{AOD} and Φ_{DRF} were even larger in the locations where NH_3 and NO_x emission rates are strong like the Central East China (CEC) region and Sichuan basin. For example, under clear-sky conditions, both Φ_{AOD} and Φ_{DRF} over the CEC region range between 6.9 % (summer) and 47.9 % (winter) and between 6.7 % (summer) and 47.5 % (winter), respectively. Based on this analysis, it was concluded that both Φ_{AOD} and Φ_{DRF} cannot be ignored in East Asian air quality and radiative forcing studies, particularly during winter.

ACPD
13, 19193–19235, 2013

1 Introduction

Ammonium nitrate (NH_4NO_3) is an important particulate constituent that is mainly produced via reversible heterogeneous reaction of gaseous ammonia (NH_3) and gaseous nitric acid (HNO_3) (i.e. $NH_3(g) + HNO_3(g) \leftrightarrow NH_4NO_3(p)$). Particulate nitrate ($NO_3^-$) can also be produced via condensation of 2 nighttime radicals (N_2O_5 and NO_3) onto aerosol particles. Particulate nitrate is then associated with ammonium (NH_4^+) formed by partitioning of gaseous NH_3. In particular, the irreversible NO_3^- formation via the condensation of N_2O_5 (i.e. $N_2O_5(g) + H_2O(p) \rightarrow 2H^+(p) + 2NO_3^-(p)$) is very active at cold temperatures. Thus, it is the dominant reaction pathway to the NH_4NO_3 production during winter.

Since NH_4NO_3 is a volatile species, its formation has been observed at locations where partial pressures or mixing ratios of NH_3 and HNO_3 are high (i.e. typically, urban and/or highly populated areas). For this reason, the NH_4NO_3 formation has been investigated over urban or highly polluted areas (e.g. Zheng et al., 2002; Kim et al., 2006), whereas it has been largely neglected in global air quality modeling studies (e.g. van Dorland et al., 1997; Chin et al., 2001; Takemura et al., 2002). In particular, many previous studies have reported that the influence of NH_4NO_3 on aerosol optical properties (AOPs) and on direct radiative forcing (DRF) by aerosols is insignificant (e.g., Andreae, 1995; van Dorland et al., 1997; Adams et al., 1999; Ramanathan et al., 2001; Chin et al., 2001; Jacobson, 2001; Takemura et al., 2002; Conant et al., 2003; Seinfeld et al., 2004; Chung et al., 2010; Zhang et al., 2012).

In particular, East Asia is highly populated and its industrial and agricultural growth rates are very high. Thus, the mixing ratios of NH_3 (emitted mainly from agricultural sector) and NO_x (emitted mainly from industrial sector; NO_x is a precursor of HNO_3) in the gas phase are high in order for the formation of NH_4NO_3 to be active. Therefore, in this manuscript, we wish to investigate whether the contribution of NH_4NO_3 to AOD and DRF by aerosols (Φ_{AOD} and Φ_{DRF}) over "East Asia" can really be negligible. If the

ACPD
13, 19193–19235, 2013

NH_4NO_3 formation is active over East Asia, then its contribution to AOD and DRF by aerosols can be of potential significance in this region.

In the above context, we attempted to answer to the following important scientific questions in this manuscript: (1) is the formation of NH_4NO_3sufficiently inactive over East Asia (particularly, over China), such that its impacts on AOD and DRF by aerosols can be ignored, despite strong emissions of its gas-phase precursors such as NH_3 and NO_x?; (2) if the NH_4NO_3formation over East Asia cannot be negligible, then how large are the influences of NH_4NO_3formation on AOD and DRF by aerosols expected to be?; (3) is there any seasonal (or temporal) variation in the production of NH_4NO_3over East Asia?; and (4) can any characteristic feature be found in the spatial distributions of NH_4NO_3 over China (strong source region of NH_3 and NO_x), as well as over the regions surrounding China, such as the Korean peninsula, Japan, and Taiwan?

2 Methods

In order to estimate the contribution of NH_4NO_3 to AOD and DRF by aerosols in East Asia, meteorological model (MM), chemistry-transport model (CTM), and radiative transport model (RTM) simulations were carried out sequentially in this study. The Fifth-Generation NCAR/Pennsylvania State Meso-scale Model (MM5) and US EPA Model-3/CMAQ (Community Multiscale Air Quality) v4.5.1 model simulations were first conducted to produce 4-dimensional (4-D) aerosol composition over an East Asian domain. The accuracy of the CMAQ model simulations was then evaluated by comparison between the particulate composition observed from the Acid Deposition Monitoring Network in East Asia (EANET) and the CMAQ-calculated particulate composition. After the evaluation, the CMAQ-calculated particulate concentrations were converted into aerosol optical properties with and without the consideration of NH_4NO_3, using a conversion algorithm. The CMAQ-estimated aerosol optical depth (AOD) was then assimilated with MODIS-retrieved AOD data in order to further improve the accuracy of the CMAQ-estimated AOD data. Finally, using the assimilated AOD data, Santa Bar-

ACPD
13, 19193–19235, 2013

bara DISORT Atmospheric Radiative Model (SBDART) simulations were conducted to calculate the DRF by aerosols with and without the consideration of NH_4NO_3 concentrations. The flow diagram of the procedures of this study is illustrated in Fig. 1. Detailed descriptions on the procedures of this study are given in the following sections.

2.1 Chemistry-transport modeling

First, we ran the US EPA CMAQ model in conjunction with MM5 for the entire year of 2006 over an East Asian domain (regarding the domain, refer to Fig. 2). In order to prepare meteorological fields for driving the CMAQ model, 2.5° × 2.5° NCEP/DOE AMIP-II Reanalysis data (Reanalysis-2) were used for the initial and boundary conditions (ICs/BCs) for the MM5 simulation. Also, in order to reduce the uncertainty of the MM5 simulation, QuikSCAT 10 m wind data (collected from the NASA/JPL SeaWinds Scatterometer aboard the QuikSCAT) were used for Four Dimensional Data Assimilation (FDDA) (Park et al., 2011a). The spatial resolution for the one-way coupled MM5-CMAQ model simulations was $30 \times 30\,km^2$, with 14 σ terrain following vertical layers. AERO4 was employed as the module for the considerations of aerosol thermodynamic/dynamic processes in the CMAQ model simulations, and SAPRC-99 and Pleim scheme were selected for the gas-phase chemistry and dry deposition, respectively (Pleim et al., 1996; Carter, 2000). In particular, thermodynamics related to the heterogeneous NH_4NO_3 formation and decomposition was treated by ISORROPIA model in the AERO4 (Nenes et al., 1998; Fountoukis and Nenes, 2007). Other details on how to run the one-way coupled MM5-CMAQ models have been explained in Park et al. (2011b).

For a more accurate chemistry-transport model simulation, the best-available emission inventories were used based on INTEX-B/EDGAR (for China, Mongolia and Russia), CAPSS (for Korea) and REAS (for Japan) inventories for "anthropogenic" emissions. The EDGAR emission was used only for the consideration of NH_3 emission in China, Mongolia and Russia, since several previous studies have shown that the INTEX-B (or ACE-ASIA) NH_3 emissions are possibly overestimated in East Asia (e.g.

ACPD
13, 19193–19235, 2013

Kim et al., 2006; Song et al., 2008). The monthly variations of the anthropogenic NO_x, SO_2, NH_3, and NMVOCs emissions were also applied in this study (Han et al., 2009; Park et al., 2011b). In addition, "biogenic" volatile organic compound (BVOC) emissions were calculated by MEGAN (Model of Emissions of Gases and Aerosols from Nature). In order to consider "geogenic" mineral dust emissions and transport, Asian Dust Aerosol Model (ADAM) simulations were also carried out in East Asia from March to May 2006. The ADAM-estimated concentrations of mineral dust were then simply added to the CMAQ-estimated particulate concentrations, based on an assumption that mineral dust particles are not significantly chemically-altered during their transboundary transport in East Asia (regarding this issue, refer to Song et al., 2005, 2007, 2012).

2.2 EANET data

EANET was organized as an international effort to enhance a general understanding of the state of acid deposition problems in East Asia; 13 countries in Asia are participating in the EANET activities. Currently, Asia Center for Air Pollution Research (ACAP) is responsible for managing the EANET (more details are described at http://www.acap.asia/profile/index4.html). While a total of 51 EANET monitoring sites are located in Asia, the observations from 12 EANET sites in our domain (1 site in Russia, 3 sites in Korea, and 8 sites in Japan) were used in this study (regarding the locations of the 12 EANET sites, refer to Fig. 2). Concentrations of 3 particulate species (NO_3^-, SO_4^{2-} and NH_4^+) from the 12 EANET sites were mainly used in this study. The 3 particulate species concentrations were measured using the filter-pack method. This filter-pack measurement has been designed for monitoring the dry deposition in East Asia. However, such 12 EANET sites are all located outside China, although 8 EANET sites have been established inside China (Guanyinqiao, Haifu, Shizhan, Jiwozi, Hongwen, Xiaoping, Xiang Zhou, and Zhuxiandong). Since the filter-pack measurements were not made in the 8 Chinese EANET sites, the particulate composition data at those 8 sites were not available. At the 8 EANET sites in China, ionic concentrations

ACPD
13, 19193–19235, 2013

in precipitation (i.e. wet scavenging) were only measured. Therefore, those sites were excluded from our consideration in this study.

The measurements from the EANET have often been used for evaluating the accuracy of chemistry-transport modeling results in East Asia (e.g., Wang et al., 2002; Choi et al., 2009; Jeong et al., 2011). The particulate concentrations of NO_3^-, SO_4^{2-}, and NH_4^+ obtained from the EANET were again used to evaluate the accuracy of CMAQ-estimated particulate concentrations in this study. The EANET data were obtained from the official EANET website at http://www.eanet.asia/product/index.html.

2.3 CMAQ-estimated aerosol optical properties

The CMAQ model simulations were carried out in order to produce the 4-D aerosol composition in the domain. Based on the particulate composition calculated via the CMAQ model simulations, AOD (τ) and single scattering albedo (SSA; ω) were sequentially estimated at a wavelength of 550 nm (hereafter, "CMAQ-estimated AOD" and "CMAQ-estimated SSA"). AOD can be theoretically calculated by integrating the aerosol extinction coefficient (σ_{ext}) with respect to altitude (z) (see Eq. 1), and columnar SSA (ω) can also be calculated using Eq. (2). In Eqs. (1) and (2), σ_{ext} and σ_{scat} are calculated via Eqs. (3)–(5), as shown below:

$$\tau = \int \sigma_{ext}(z) \cdot dz \quad (1)$$

$$\omega = \frac{\int \sigma_{scat}(z) \cdot dz}{\tau} \quad (2)$$

$$\sigma_{ext} = \sigma_{scat} + \sigma_{abs} \quad (3)$$

$$\sigma_{scat}(M\,m^{-1}) \approx 3.0 \times f(RH) \times \{[(NH_4)_2SO_4] + [NH_4NO_3]\} + \omega_{EC} \times 10.0 \times [Elemental\_Carbon] + \sum_i^n \{\omega_{dust,i} \times \beta_i \times [Dust]_i\} + 4.0 \times [Organic\_Mass] + 1.37 \times f_{ss}(RH) \times [Sea\_Salt] \quad (4)$$

ACPD
13, 19193–19235, 2013

$$\sigma_{abs}(\mathrm{M\,m^{-1}}) \approx (1-\omega_{EC}) \times 10.0 \times [\mathrm{Elemental\_Carbon}] + \sum_{i}^{n} \{(1-\omega_{dust,i}) \times \beta_i \times [\mathrm{Dust}]_i\} \quad (5)$$

where $f(\mathrm{RH})$ represents the hygroscopic growth factors of $(NH_4)_2SO_4$ and NH_4NO_3, and $f_{ss}(\mathrm{RH})$ also represents that of sea-salt particles. These factors are a function of relative humidity (RH). In order to calculate CMAQ-estimated AOD and SSA without the consideration of NH_4NO_3 in this study, the term "NH_4NO_3" was removed from Eq. (4).

2.4 Data assimilation

The AOD data at 550 nm was also retrieved from MODIS sensor onboard Terra satellite (we label this "MODIS-retrieved AOD"). Then, the MODIS-retrieved AOD was assimilated, using the CMAQ-estimated AOD, in order to produce the best accurate and temporally/spatially continuous sets of the AOD data over East Asia (hereafter, we label this product "assimilated AOD"). This approach is designed to maximize the advantages (and also to minimize the drawbacks) of the CMAQ-estimated and MODIS-retrieved AOD data sets: the CMAQ-estimated AOD data, spatially and temporally continuous (i.e. four dimensionally continuous), is not affected by the presence of clouds and high surface albedo, but is believed to be less accurate. In contrast, the MODIS-retrieved AOD data is spatially and temporally discontinuous, depending on the presence of clouds and high surface albedo, but is believed to be more accurate than the CMAQ-estimated AOD. Therefore, we combined the two AOD data sets via a data assimilation technique, called optimal interpolation (OI) with Kalman gain matrix. The expressions for the OI and Kalman gain matrix are shown in Eqs. (6) and (7):

$$\tau'_m = \tau_m + \mathbf{K}(\tau_o - H\tau_m) \quad (6)$$

$$\mathbf{K} = BH^T(HBH^T + O)^{-1} \quad (7)$$

ACPD
13, 19193–19235, 2013

where τ_o and τ_m represent the MODIS-retrieved and CMAQ-estimated AODs, respectively. H denotes the linear operator for interpolation from the model grid to the location of the observations, and **K** is the Kalman gain matrix (or Kalman filter). The Kalman gain matrix was calculated by applying seasonally-variable free parameters in order to improve the efficiency of the OI in this study (Park et al., 2011b). For the 2 case studies with and without NH_4NO_3, the data assimilation was performed with the same free parameters.

2.5 AERONET AOD and DRF by aerosols

In order to confirm the accuracy of the assimilated AOD data, the monthly-averaged assimilated AOD values were compared with monthly-averaged AERONET AOD values at the wavelength of 550 nm. In addition, the DRF by aerosols was also calculated, and the monthly-averaged DRF by aerosols were then compared with the monthly-averaged DRF values from 8 AERONET sites. The AERONET DRF values were downloaded from the AERONET web site at http://aeronet.gsfc.nasa.gov/. Level 2.0 dataset from the AERONET web site was used in this study. The AERONET DRF values by aerosols were calculated using AERONET inversion code that is a corresponding module of radiative forcing model, GAME (Global Atmospheric ModEl) (Dubuisson et al., 1996; Roger et al., 2006). This model performs spectral integration using correlated-k distribution, based on line-by-line simulations (Scott, 1974). The correlated-k distribution takes into account the interactions between gaseous absorption and multiple scattering with manageable computational time (Garcia et al., 2008); this module is thus believed to accurately account for the molecular scattering and gaseous absorption effects (Garcia et al., 2012).

2.6 Radiative transport modeling

The estimations of the DRF by aerosols with assimilated and model-calculated aerosol optical property data were made via Santa Barbara DISORT Atmospheric Radiative

ACPD
13, 19193–19235, 2013

Model (SBDART). This model was developed at the University of California, Santa Barbara, following Ricchiazzi et al.'s method (1998). The SBDART is a plane-parallel model that computes the transfer of radiation through 40 layers from the earth surface to the top of the atmosphere. The SBDART has been widely used to date for the analysis of radiative forcing as well as atmospheric energy budget studies (e.g. Xia and Zong, 2009; Ge et al., 2010; Lin et al., 2013; Sena et al., 2013).

The important parameters for the estimations of DRF by aerosols are the AOD, single scattering albedo (SSA), asymmetry factor (g), surface albedo, and profiles of atmospheric parameters (such as temperature, humidity, ozone, and trace gases). In this study, we assumed the US62 standard atmosphere (US Standard Atmosphere, 1962). Again, the AOD values utilized in this study were improved by the assimilation procedures, and the SSA values calculated from the CMAQ model simulations were evaluated with the values from AERONET and LiDAR network (ADNET) in East Asia (regarding this work, refer to Park et al., 2011b). The monthly-averaged asymmetry factor (g) was retrieved from AERONET and was then used for the SBDART simulations in this study. The mean value of g at the AERONET sites (data from 9 sites were available) converged into 0.69 with small standard deviations (see Fig. 3). Therefore, this asymmetric factor of 0.69 was utilized in the SBDART simulations. In addition, the data of surface albedo over East Asia was obtained from European Center for Medium-Range Weather Forecasts (ECMWF).

In addition, cloud information such as cloud optical depth (COD), cloud height, and cloud fraction is necessary in order to calculate the DRF by aerosols under cloudy (all-sky) conditions. Such cloud information was obtained from the MODIS sensor onboard Terra satellite in this study. The cloud top height was converted from cloud top pressure using state equation and the cloud bottom height was assumed to be 200 m above the surface following the assumption of the SCIAMACHY retrieval procedure (regarding this issue, refer to http://www.sciamachy.org/products/clouds/clouds_IFE_PSD.pdf). The cloud information was then used as input data to the SBDART model simulations under all-sky conditions.

ACPD
13, 19193–19235, 2013

The DRF by aerosols at the top of atmosphere, denoted as ΔF_{TOA}, is defined as the difference between solar irradiances with and without particular particulate species in Eq. (8):

$$\Delta F_{TOA} = -\left(F^{a}_{TOA} - F^{0}_{TOA}\right) \quad (8)$$

where, F^{a}_{TOA} and F^{0}_{TOA} represent the broadband fluxes with and without particular particulate species, respectively. The contributions of NH_4NO_3 to DRF (Φ_{DRF}) were estimated from the differences between the DRF values calculated with and without NH_4NO_3 in this study. For the comparison with the AERONET DRF values, the SBDART-estimated DRF values were calculated under clear-sky conditions, because the AOD and DRF data from AERONET during cloudy days were screened out. The estimations of DRF by aerosols under clear-sky and all-sky conditions were also made in order to investigate the Φ_{DRF} in this study (see Sect. 3.3).

3 Results and discussions

3.1 Evaluation of CMAQ-estimated particulate concentrations

First, in order to confirm the accuracy of the CMAQ-estimated particulate concentrations, a comparative analysis between CMAQ-estimated and EANET-derived particulate concentrations was conducted. In Figs. 4–6, the CMAQ-estimated particulate concentrations of NO_3^-, SO_4^{2-}, and NH_4^+ were compared with the EANET-derived particulate concentrations at the 12 EANET sites for 12 months of 2006. In this study, focus was given to 3 particulate species, NO_3^-, SO_4^{2-}, and NH_4^+, because they are the main constituents of atmospheric aerosols in East Asia. Also, other particulate species such as black carbon (BC) and organic aerosols (OAs) were not measured in the EANET activities, partly because these species are not directly related to acid deposition in East Asia.

ACPD
13, 19193–19235, 2013

The CMAQ-estimated concentrations of NO_3^-, SO_4^{2-}, and NH_4^+ showed good agreements with the EANET NO_3^-, SO_4^{2-}, and NH_4^+ concentrations (Figs. 4–6). In Fig. 4, the monthly variation of NO_3^- showed high values during winter. Such high NO_3^- concentrations during the winter season are mainly due to the active formation of NH_4NO_3 at cold temperatures (i.e. via 2 active heterogeneous reactions in winter: (1) $NH_3(g) + HNO_3(g) \rightarrow NH_4NO_3(p)$ and (2) $N_2O_5(g) + H_2O(p) \rightarrow 2H^+(p) + 2NO_3^-(p)$). In contrast, the monthly variation of SO_4^{2-} showed slightly high values during summer (Fig. 5), partly because of the active formation of $(NH_4)_2SO_4$ at high temperature. As mentioned in Sect. 1, the sulfate and nitrate formations are active in urban areas and are less active in remote and rural areas. However, the concentrations of NO_3^-, SO_4^{2-}, and NH_4^+ at the Cheju, Imsil, and Kanghwa sites (although they are remote and/or rural areas) were comparable to or higher than those at the Banryu site (urban area) as shown in Figs. 4–6. In particular, the concentrations of NO_3^-, SO_4^{2-}, and NH_4^+ at such remote and rural areas during spring, fall, and winter were large. This could be somehow related to the long-range transport of both particulate species and their precursors from China to the Korean EANET sites.

In the spring, fall and winter seasons, the wind patterns are typically very favorable for the long-range transport of air pollutants from China to the Korean peninsula and Japan due to persistent westerly and northwesterly winds in East Asia. In contrast, the surface wind patterns in East Asia are affected by the East Asian monsoon during summer, causing southeasterly winds on the surface during summer. Seasonally-averaged surface wind vectors are shown in Fig. 7, using the NCEP/NCAR reanalysis dataset. Based on such seasonal variations of the surface wind patterns in East Asia, transboundary air pollution from China to Korea and Japan could be minimized during summer. Collectively, the highly-polluted air masses in China can be more efficiently transported to the Korean peninsula and the Japan islands during spring, fall, and winter, and the unexpected high concentrations of NO_3^-, SO_4^{2-}, and NH_4^+ observed at the 3 Korean remote and rural EANET sites during spring, fall, and winter can be explained

ACPD
13, 19193–19235, 2013

by these seasonal variations of the surface wind patterns in East Asia. In addition, as shown in Fig. 5, the summer SO_4^{2-} peaks are not particularly distinctive. This is also partly due to the inactive long-distance transport of SO_4^{2-} from China to the Korean peninsula and Japan in summer. In other words, the SO_4^{2-} concentrations in Fig. 5 during spring, fall, and winter are not only photochemically produced, but are also influenced by the long-range transport.

Some statistical analyses between the CMAQ-estimated and EANET-derived particulate NO_3^-, SO_4^{2-}, and NH_4^+ concentrations were conducted (scatter plot analysis in Fig. 8 and error and bias analysis in Table 1). In Table 1, the statistical values of R, χ^2, RMSE, MNGE, MB, and MNB were analyzed, and the definitions and abbreviations of the statistical variables are presented in the footnote of Table 1. As shown in Fig. 8 and Table 1, NO_3^- and NH_4^+ show slight positive biases (i.e. CMAQ overestimation), whereas SO_4^{2-} shows negative biases (i.e. CMAQ underprediction). In particular, relatively large RMSEs with the negative biases in SO_4^{2-} are found, compared to those in NO_3^- and NH_4^+, as also shown in Figs. 4–6. These large RMSEs with the negative biases in SO_4^{2-} can result in under-prediction of CMAQ-estimated AODs, compared to the AERONET AOD in Fig. 10. This will be further discussed in Sect. 3.2.

It is also worthwhile to note that large parts of the errors and biases mainly occurred at the 3 Korean EANET sites: Cheju, Imsil, and Kwanghwa, as shown in Figs. 4–6. The relatively large errors and biases in the NO_3^-, SO_4^{2-}, and NH_4^+ concentrations at the 3 Korean sites could be partly caused by the uncertainties in the NO_x, SO_2, and NH_3 emissions used in Korea. As mentioned previously, the INTEX-B/EDGAR, CAPSS, and REAS inventories were used for the anthropogenic NO_x, SO_2, and NH_3 emissions over China, Korea, and Japan, respectively. The large RMSEs and biases derived from the Korean EANET sites could be due to the relatively large uncertainty in the CAPSS emissions (although the Korean EANET sites can also be influenced by the uncertainty in the INTEX-B/EDGAR emissions over China via the long-range transport of those particulate species). In contrast, the relatively good correlations between the

ACPD
13, 19193–19235, 2013

CMAQ-estimated and EANET-derived particulate concentrations of NO_3^-, SO_4^{2-}, and NH_4^+ at the 8 Japanese sites reflect the relatively high accuracies of NO_x, SO_2, and NH_3 emissions from the REAS inventory. Although the CMAQ-estimated particulate concentrations of NO_3^-, SO_4^{2-}, and NH_4^+ have some errors and biases compared to the EANET data, there are in general good agreements between the CMAQ-calculated particulate composition and the EANET data, based on the statistical analysis.

In addition, the mass ratios of the NH_4NO_3 ($R_{NO_3/PM_{2.5}}$ and $R_{NO_3/PM_{10}}$) and $(NH_4)_2SO_4$ ($R_{SO_4/PM_{2.5}}$ and $R_{SO_4/PM_{10}}$) concentrations to $PM_{2.5}$ and PM_{10} were calculated from the CMAQ model simulations in East Asia for the entire year of 2006. The annual average values of $R_{NO_3/PM_{2.5}}$ and $R_{NO_3/PM_{10}}$ were 0.17 and 0.14, respectively. The fractions are smaller than the values of $R_{SO_4/PM_{2.5}}$ (0.25) and $R_{SO_4/PM_{10}}$ (0.20). Monthly variations of $R_{NO_3/PM_{2.5}}$, $R_{NO_3/PM_{10}}$, $R_{SO_4/PM_{2.5}}$, and $R_{SO_4/PM_{10}}$ are presented in Fig. 9. As expected, $R_{NO_3/PM_{2.5}}$ and $R_{NO_3/PM_{10}}$ show the highest values in winter, whereas $R_{SO_4/PM_{2.5}}$ and $R_{SO_4/PM_{10}}$ show their maxima in summer. This analysis indicates that the mass contributions of NH_4NO_3 to particulate matter are almost comparable to those of $(NH_4)_2SO_4$ in East Asia. The $R_{NO_3/PM_{2.5}}$ and $R_{NO_3/PM_{10}}$ values (blue lines) are even larger than the $R_{SO_4/PM_{2.5}}$ and $R_{SO_4/PM_{10}}$ values (red lines) during winter, as shown in Fig. 9. In terms of the mass fraction, NH_4NO_3 cannot be ignored in East Asia, particularly during winter. In this context, the contribution of NH_4NO_3 to AOD and DRF in East Asia will be further investigated in Sects. 3.2 and 3.3.

3.2 Contribution of ammonium nitrate to AOD in East Asia

The monthly-averaged AOD products from AERONET and two assimilated AODs (with and without NH_4NO_3) were compared in Fig. 10 at 8 AERONET sites, in order to confirm the accuracy of the assimilated AOD and in order to evaluate the impact of NH_4NO_3 on AOD. In this analysis, the AERONET AOD was regarded as reference value ("ground truth"), since it is not interfered by the surface reflectance and the level 2.0 AERONET data is well-calibrated (Holben et al., 1998; Dubovik et al., 2000). The

ACPD
13, 19193–19235, 2013

locations of the 8 AERONET sites are presented in Fig. 2. As shown in Fig. 2, four pairs of AERONET sites are located in China (near Beijing), Korea, Japan, and Taiwan, respectively. This selection of the AERONET sites was made, based on the availability (or scarcity) of data. As shown in Fig. 10, there are relatively good agreements between monthly-averaged AERONET AODs and monthly-averaged assimilated AODs with NH_4NO_3 (blue-dotted lines), showing correlation coefficients (Rs) ranging from 0.71 to 0.91 and root mean square errors (RMSEs) ranging from 0.08 to 0.21. In contrast, the degree of agreements decreased, when monthly-averaged AERONET AODs are compared with monthly-averaged assimilated AODs without NH_4NO_3 (red-dotted lines). In this case, Rs and RMSEs ranged between 0.45 and 0.91 and between 0.04 and 0.41, respectively. As presented in Fig. 10, the AOD values with NH_4NO_3 (blue-dotted lines) are closer to AERONET AOD (gray bars) than the AOD values without NH_4NO_3 (red-dotted lines).

It should also be noted here that the monthly-averaged assimilated AOD values (blue dotted lines) are in general underestimated, compared with the AERONET AOD values, as shown in Fig. 10. These underestimations (or discrepancies) can be affected by several factors: (1) uncertainties in the magnitudes and monthly variations of the emission rates of the gas-phase precursors of particulate species (e.g. Kim et al., 2006; Song et al., 2008; Zheng et al., 2012); (2) underestimation of SO_4^{2-} concentrations, as shown in Figs. 5 and 8; (3) possible underestimation of concentrations of black carbon (BC) and organic aerosols (OAs) (Volkamer et al., 2006; Carlton et al., 2009; Kim et al., 2012); and (4) uncertainties in the one-way coupled MM5-CMAQ model simulations and the composition-to-AOD conversion algorithm (Kinne et al., 2003; Zhang et al., 2006; Park et al., 2011b).

The differences between the monthly-averaged AOD values with and without NH_4NO_3 vary spatially and seasonally. In Fig. 11, the monthly-averaged AOD values with and without NH_4NO_3 over 6 specific regions (CEC, Sichuan, Guangdong, Korea, Japan, and Taiwan; refer to Fig. 2) were calculated (see blue and red dotted lines), and were then compared with the MODIS-retrieved AOD values (see gray bars in Fig. 11),

ACPD
13, 19193–19235, 2013

in order to investigate the regional influences of NH_4NO_3 on the AOD values. The differences between the blue and red dotted lines are the largest in the 3 Chinese regions (CEC, Sichuan, and Guangdong) and are also relatively large in Korea. However, the differences in the other two regions (Japan and Taiwan) are almost negligible. The largest differences in the 3 Chinese regions are due to more active formation of NH_4NO_3 over the Chinese regions than over other regions, because the CEC, Sichuan, and Guangdong regions are highly polluted and emit large amounts of NO_x and NH_3. Especially, NH_4NO_3 over the Sichuan region is not efficiently dispersed, because the Sichuan basin is surrounded by tall mountains. The relatively large differences between the AOD values with and without NH_4NO_3 in Korea could also be transferred from the CEC region via the long-range transport of particulate species and their precursors due to the proximity between CEC and Korea (refer to Figs. 2 and 7). Also, the differences are larger during cold months (such as December, January, February and March) in Figs. 10 and 11. This is due to the fact that the equilibrium between gas-phase NH_3/HNO_3 and particulate NH_4NO_3 tends to shift toward a more active formation of NH_4NO_3 with colder temperature ($NH_3(g) + HNO_3(g) \Leftrightarrow NH_4NO_3(p)$). Also, the condensation of N_2O_5 radicals onto atmospheric aerosols is particularly active during winter.

In addition to AOD, the CMAQ-estimated SSAs were also calculated with and without the consideration of NH_4NO_3 using Eqs. (2)–(5). The annual average SSA values calculated from the CMAQ model simulations show almost negligible differences between the cases with and without the consideration of NH_4NO_3 (0.97 and 0.96, respectively). The differences also show a seasonal variation, ranging from 0.0 (summer) to 0.02 (winter). These CMAQ-estimated SSAs were used for the calculations of the DRF by aerosols in East Asia that will be discussed in next section (Sect. 3.3).

3.3 Contribution of ammonium nitrate to DRF by aerosols in East Asia

As discussed in the previous section, the monthly-averaged DRF by aerosols from AERONET were compared with the monthly-averaged DRF estimated from the SB-

ACPD
13, 19193–19235, 2013

DART at the 8 AERONET sites (see Fig. 12). Again, there were relatively good agreements between the DRF from AERONET and the DRF estimated by the SBDART simulations (i.e. gray bars vs. blue-dotted lines in Fig. 12). Also, some differences between the two SBDART-derived DRFs with and without NH_4NO_3 were observed (i.e. blue-dotted lines vs. red-dotted lines). The differences are again the largest at the two Chinese AERONET sites and also during the cold months. However, even during the cold months, there are almost no differences in the AOD and DRF values at Japanese and Taiwan sites, as shown in Figs. 10 and 12. This is due to the fact that the formation of NH_4NO_3 is not very active in Japan and Taiwan, because of (1) relatively low levels of NH_3 and NO_x and (2) relatively warm temperature over those locations. This is also shown in Figs. 13 and 14.

Based on the analysis shown in Fig. 12, two-dimensional calculations of DRF by aerosols over the entire East Asian domain were made. Figure 13 shows the spatial distribution of the DRF by aerosols estimated from the SBDART simulations over East Asia for four seasons of 2006 under clear-sky conditions. As shown in Figs. 10–12, the formation of NH_4NO_3 is the most active in winter and spring, and hence the differences in the DRF values (the third column) between the cases with and without NH_4NO_3 (the first and second columns in Fig. 13) are the largest in the cold seasons (also, refer to the domain-averaged values of the DRF by aerosols for the two cases in Fig. 13).

The differences are particularly large in the regions where NH_3 and NO_x emission rates are strong over the CEC region and the Sichuan basin. The strong NH_3 and NO_x emissions result in high levels of gas-phase NH_3 and HNO_3, which again lead to active formation of NH_4NO_3 over these locations. The spatial distributions of the NH_3 and NO_x emissions are shown in Fig. 14. According to Fig. 14, the Guangdong region (including Hong Kong and Guangzhou) is also strong source of NH_3 and NO_x, but the formation of NH_4NO_3 is less active over this region than over the Sichuan basin and the CEC region, due to relatively warm temperature. The differences in the DRF between the cases with and without NH_4NO_3, reach $-35\,W\,m^{-2}$ over the CEC region and Sichuan basin during winter. Therefore, collectively, the impacts of NH_4NO_3 on AOD and DRF

ACPD
13, 19193–19235, 2013

by aerosols should not be ignored, particularly over East Asia where both NH_3 and NO_x emission rates are strong.

In addition, it is also noteworthy that there are relatively large uncertainties in the NH_3 and NO_x emissions in East Asia (refer to Kim et al., 2006; Song et al., 2008; Han et al., 2009). As discussed previously, these uncertainties can lead to inaccurate estimation of NH_4NO_3 concentrations. Therefore, there is a possibility that the discrepancies shown in Figs. 10–12 can be caused by these uncertainties over East Asia. For a more accurate estimation of NH_4NO_3 concentrations in East Asia, improvements in the NH_3 and NO_x emission rates should be made in the future.

The DRF by aerosols under all-sky conditions was also calculated in Fig. 15. The domain-averaged values of the DRF by aerosols under all-sky conditions were smaller than those under clear-sky conditions, because large fraction of sunlight was scattered by the presence of clouds. In particular, over the Sichuan basin, the DRF by aerosols under all-sky conditions became small, although the DRF by aerosols under clear-sky conditions was large. Such large differences in the DRF by aerosols between under clear-sky and all-sky conditions were related to the large annual mean values of CODs and cloud fractions over the Sichuan basin (regarding this issue, refer to Fig. S1 in the Supplement).

Both Φ_{AOD} and Φ_{DRF} are summarized in Table 2. The contributions were calculated at the 8 AERONET sites and over the entire East Asian domain (the numbers in the first parentheses of Table 2 represent domain-averaged values). Both Φ_{AOD} and Φ_{DRF} over East Asia vary seasonally with the ranges between 4.7 % (summer) and 31.3 % (winter) and between 4.7 % (summer) and 30.7 % (winter), respectively under clear-sky conditions, showing annual average contributions of 15.6 % and 15.3 %. Under all-sky conditions, Φ_{DRF} varied between 3.6 % (summer) and 24.5 % (winter), showing annual average contribution of 12.1 % over East Asia. These annual average Φ_{AOD} and Φ_{DRF} are almost comparable to the annual average mass fractions of NH_4NO_3 to $PM_{2.5}$ and PM_{10} (17.0 % and 14.0 %, respectively). Φ_{AOD} and Φ_{DRF} become larger in the locations where NH_3 and NO_x emission rates are strong such as in the CEC region

ACPD
13, 19193–19235, 2013

and Sichuan basin. For example, under clear-sky conditions, both Φ_{AOD} and Φ_{DRF} over the CEC region range between 6.9 % (summer) and 47.9 % (winter) and between 6.7 % (summer) and 47.5 % (winter), respectively, showing annual average contributions of 23.3 % and 22.8 %. However, these contributions (Φ_{AOD} and Φ_{DRF}) decrease over the regions surrounding China: Korean peninsula (19.4 % and 19.6 %), Japan (10.7 % and 10.9 %), and Taiwan (5.4 % and 5.5 %), as shown in Table 2. Under all-sky conditions, the annual average values of Φ_{DRF} were found to be 21.0 % over the CEC region, 15.6 % over the Korean peninsula, 8.5 % over Japan, and 3.1 % over Taiwan. Based on this analysis, it can be said that Φ_{AOD} and Φ_{DRF} are so large particularly during the winter season over East Asia that they cannot be ignored in the East Asian air quality and radiative forcing studies.

4 Conclusions and outlook

In this study, the contribution of NH_4NO_3 to AOD and DRF by aerosols (Φ_{AOD} and Φ_{DRF}) over East Asia was investigated. In order to evaluate the accuracy of CMAQ-calculated particulate concentrations, the CMAQ-calculated particulate concentrations were compared with those from the EANET. Although some errors and biases between the two particulate concentrations were found, relatively good agreements are shown between the two datasets. For improvement of the accuracy of the AOD data, CMAQ-calculated AOD was assimilated, using MODIS-derived AOD, over East Asia for the entire year of 2006. After the assimilation, seasonally-varying DRF by aerosols over East Asia was estimated using the assimilated and model-calculated aerosol optical properties via a radiative transfer model, SBDART. The assimilated AOD and estimated DRF by aerosols showed nice agreements with the AOD and DRF by aerosols from AERONET. Based on these results, both Φ_{AOD} and Φ_{DRF} were estimated over East Asia for four seasons in 2006 under clear-sky and all-sky conditions. It was found from the analysis that during the cold months Φ_{AOD} and Φ_{DRF} are large. Both Φ_{AOD} and Φ_{DRF} vary seasonally with ranges between 4.7 % (summer) and 31.3 % (winter) and

ACPD
13, 19193–19235, 2013

between 4.7 % (summer) and 30.7 % (winter) over East Asia under clear-sky conditions, respectively. Under all-sky conditions, Φ_{DRF} varied between 3.6 % (summer) and 24.5 % (winter), showing annual average contribution of 12.1 % over East Asia. However, these Φ_{AOD} and Φ_{DRF} become even larger in the locations where NH_3 and NO_x emission rates are strong, such as in Central East China and Sichuan regions. For example, under clear-sky conditions, Φ_{DRF} changes between 10.9 % (summer) and 65.1 % (winter) at the two Chinese AERONET sites near Beijing. Based on this analysis, it can be said that Φ_{AOD} and Φ_{DRF} are so large particularly during the winter season over East Asia, that they cannot be ignored in the East Asian air quality and radiative forcing studies.

Furthermore, recent studies have reported that the global contributions of NH_4NO_3 to AOD and DRF by aerosols are expected to become comparable to those of $(NH_4)_2SO_4$ in the near future, since the atmospheric burden of NH_4NO_3 is increasing; however, the burden of $(NH_4)_2SO_4$ is decreasing continuously (Nakicenovic et al., 2000; Bauer et al., 2007; Bellouin et al., 2011). This is particularly true for East Asia. Therefore, we have to keep monitoring the contributions of NH_4NO_3 to AOD and DRF by aerosols over East Asia.

Supplementary material related to this article is available online at: http://www.atmos-chem-phys-discuss.net/13/19193/2013/acpd-13-19193-2013-supplement.pdf.

Acknowledgements. This research was supported by Korea Ministry of Environment as "The Eco-Innovation project" (411-113-013) in Korea, by the Korean Meteorological Administration Research and Development Program under grant CATER 2012-7110 in Korea and by the GEMS program of the Ministry of Environment, Korea and the Eco Innovation Program of KEITI (2012000160004). In this study, MODIS-retrieved aerosol data was obtained from http://ladsweb.nascom.nasa.gov/data/search.html.

ACPD
13, 19193–19235, 2013

References

Adams, P. J., Seinfeld, J. H., and Koch, D. M.: Global concentration of tropospheric sulfate, nitrate, and ammonium aerosol simulated in a general circulation model, J. Geophys. Res., 104, 13791–13823, 1999.

Andreae, M. O.: Climatic effects of changing atmospheric aerosol levels, in: World Survey of Climatology: Future Climates of the World, vol. 16, edited by: Henderson-Sellers, A., Elsevier, Amsterdam, 341–392, 1995.

Bauer, S. E., Koch, D., Unger, N., Metzger, S. M., Shindell, D. T., and Streets, D. G.: Nitrate aerosols today and in 2030: a global simulation including aerosols and tropospheric ozone, Atmos. Chem. Phys., 7, 5043–5059, doi:10.5194/acp-7-5043-2007, 2007.

Bellouin, N., Rae, J., Jones, A., Johnson, C., Haywood, J., and Boucher, O.: Aerosol forcing in the Climate Model Intercomparison Project (CMIP5) simulations by HadGEM2-ES and the role of ammonium nitrate, J. Geophys. Res., 116, D20206, doi:10.1029/2011JD016074, 2011.

Carlton, A. G., Wiedinmyer, C., and Kroll, J. H.: A review of Secondary Organic Aerosol (SOA) formation from isoprene, Atmos. Chem. Phys., 9, 4987–5005, doi:10.5194/acp-9-4987-2009, 2009.

Carter, W. P. L.: Implementation of the SAPRC-99 Chemical Mechanism into the Models-3 Framework, Report to the United States Environmental Protection Agency, available at: http://www.cert.ucr.edu/~carter/pubs/s99mod3.pdf (last access: 19 July 2013), 2000.

Chin, M., Ginoux, P., Kinne, S., Torres, O., Holben, B. N., Duncan, B. N., Martin, R. V., Logan, J. A., Higurashi, A., and Nakajima, T.: Tropospheric aerosol optical thickness from the GOCART model and comparisons with satellite and sun photometer measurements, J. Atmos. Sci., 59, 461–483, 2001.

Choi, Y.-S., Park, R. J., and Ho, C.-H.: Estimates of ground-level aerosol mass concentrations using a chemical transport model with Moderate Resolution Imaging Spectroradiometer (MODIS) aerosol observations over East Asia, J. Geophys. Res., 114, D04204, doi:10.1029/2008JD011041, 2009.

Chung, C. E., Ramanathan, V., Carmichael, G., Kulkarni, S., Tang, Y., Adhikary, B., Leung, L. R., and Qian, Y.: Anthropogenic aerosol radiative forcing in Asia derived from regional models with atmospheric and aerosol data assimilation, Atmos. Chem. Phys., 10, 6007–6024, doi:10.5194/acp-10-6007-2010, 2010.

ACPD
13, 19193–19235, 2013

Conant, W. C., Seinfeld, J. H., Wang, J., Carmichael, G. R., Tang, Y., Uno, I., Flatau, P. J., Markowicz, K. M., and Quinn, P. K.: A model for the radiative forcing during ACE-Asia derived from CIRPAS Twin Otter and R/V *Ronald H. Brown* data and comparison with observations, J. Geophys. Res., 108, 8661, doi:10.1029/2002JD003260, 2003.

Dubuisson, P., Buriez, J. C., and Fouquart, Y.: High spectral resolution solar radiative transfer in absorbing and scattering media: application to the satellite simulation, J. Quant. Spectrosc. Ra., 55, 103–126, 1996.

Dubovik, O., Smirnov, A., Holben, B. N., King, M. D., Kaufman, Y. J., Eck, T. F., and Slutsker, I.: Accuracy assessments of aerosol optical properties retrieved from Aerosol Robotic Network (AERONET) Sun and sky radiance measurements, J. Geophys. Res., 105, 9791–9806, doi:10.1029/2000JD900040, 2000.

Fountoukis, C. and Nenes, A.: ISORROPIA II: a computationally efficient thermodynamic equilibrium model for K^+–Ca^{2+}–Mg^{2+}–NH_4^+–Na^+–SO_4^{2-}–NO_3^-–Cl^-–H_2O aerosols, Atmos. Chem. Phys., 7, 4639–4659, doi:10.5194/acp-7-4639-2007, 2007.

Garcia, O. E., Diaz, A. M., Exposito, F. J., Diaz, J. P., Dubovik, O., Dubuisson, P., Roger, J.-C., Eck, T. F., Sinyuk, A., Derimian, Y., Dutton, E. G., Schafer, J. S., Holben, B., and Garcia, C. A.: Validation of AERONET estimates of atmospheric solar fluxes and aerosol radiative forcing by ground-based broadband measurements, J. Geophys. Res., 113, D21207, doi:10.1029/2008JD010211, 2008.

García, O. E., Díaz, J. P., Expósito, F. J., Díaz, A. M., Dubovik, O., Derimian, Y., Dubuisson, P., and Roger, J.-C.: Shortwave radiative forcing and efficiency of key aerosol types using AERONET data, Atmos. Chem. Phys., 12, 5129–5145, doi:10.5194/acp-12-5129-2012, 2012.

Ge, J. M., Su, J., Ackerman, T. P., Fu, Q., Huang, J. P., and Shi, J. S.: Dust aerosol optical properties retrieval and radiative forcing over northwestern China during the 2008 China-US joint field experiment, J. Geophys. Res., 115, D00K12, doi:10.1029/2009JD013263, 2010.

Han, K. M., Song, C. H., Ahn, H. J., Park, R. S., Woo, J. H., Lee, C. K., Richter, A., Burrows, J. P., Kim, J. Y., and Hong, J. H.: Investigation of NO_x emissions and NO_x-related chemistry in East Asia using CMAQ-predicted and GOME-derived NO_2 columns, Atmos. Chem. Phys., 9, 1017–1036, doi:10.5194/acp-9-1017-2009, 2009.

Holben, B. N., Eck, T. F., Slutsker, I., Tanré, D., Buis, J. P., Setzer, A., Vermote, E., Reagan, J. A., Kaufman, Y. J., Nakajima, T., Lavenu, F., Jankowiak, I., and Smirnov, A.: AERONET – a fed-

ACPD
13, 19193–19235, 2013

erated instrument network and data archive for aerosol characterization, Remote Sens. Environ., 66, 1–16, 1998.
Jacobson, M. Z.: Global direct radiative forcing due to multicomponent anthropogenic and natural aerosols, J. Geophys. Res., 106, 1551–1568, doi:10.1029/2000JD900514, 2001.
Jeong, J. I., Park, R. J., Woo, J.-H., Han, Y.-J., and Yi, S.-M.: Source contributions to carbonaceous aerosol concentrations in Korea, Atmos. Environ., 45, 1116–1125, 2011.
Kim, J. Y., Song, C. H., Ghim, Y. S., Won, J. G., Yoon, S. C., Carmichael, G. R., and Woo, J.-H.: An investigation on NH_3 emissions and particulate NH_4^+–NO_3^- formation in East Asia, Atmos. Environ., 40, 2139–2150, 2006.
Kim, M. Y., Lee, S. B., Bae, G. N., Park, S. S., Han, K. M., Park, R. S., Song, C. H., and Park, S. H.: Distribution and direct radiative forcing of black carbon aerosols over Korean Peninsula, Atmos. Environ., 58, 45–55, 2012.
Kinne, S., Lohmann, U., Feichter, J., Schulz, M., Timmreck, C., Ghan, S., Easter, R., Chin, M., Ginoux, P., Takemura, T., Tegen, I., Koch, D., Herzog, M., Penner, J., Pitari, G., Holben, B., Eck, T., Smirnov, A., Dubovik, O., Slutsker, I., Tanre, D., Torres, O., Mishchenko, M., Geogdzhayev, I., Chu, D. A., and Kaufman, Y.: Monthly averages of aerosol properties: a global comparison among models, satellite data, and AERONET ground data, J. Geophys. Res., 108, 4634, doi:10.1029/2001JD001253, 2003.
Lin, L., Fu, Q., Zhang, H., Su, J., Yang, Q., and Sun, Z.: Upward mass fluxes in tropical upper troposphere and lower stratosphere derived from radiative transfer calculations, J. Quant. Spectrosc. Ra., 117, 114–122, 2013.
Nakicenovic, N., Davidson, O., Davis, G., Grübler, A., Kram, T., Lebre La Rovere, E., Metz, B., Morita, T., Pepper, W., Pitcher, H., Sankovski, A., Shukla, P., Swart, R., Watson, R., and Dadi, Z. (eds.): Emissions Scenarios – Summary for Policymakers. A Special Report of Working Group III of the Intergovernmental Panel on Climate Change (IPCC), IPCC, Geneva, Switzerland, 20 pp., 2000.
Nenes, A., Pandis, S. N., and Pilinis, C.: ISORROPIA: a new thermodynamic equilibrium model for multiphase multi-component inorganic aerosols, Aquat. Geochem., 4, 123–152, 1998.
Park, R. S., Cho., Y.-K., Choi, B.-J., and Song, C. H.: Implications of sea surface temperature deviations in the prediction of wind and precipitable water over the Yellow Sea, J. Geophys. Res., 116, D17106, doi:10.1029/2011JD016191, 2011a.
Park, R. S., Song, C. H., Han, K. M., Park, M. E., Lee, S.-S., Kim, S.-B., and Shimizu, A.: A study on the aerosol optical properties over East Asia using a combination of CMAQ-simulated

ACPD
13, 19193–19235, 2013

aerosol optical properties and remote-sensing data via a data assimilation technique, Atmos. Chem. Phys., 11, 12275–12296, doi:10.5194/acp-11-12275-2011, 2011b.

Pleim, J. E., Clarke, J. E., Finkelstein, P. L., Cooter, E. J., Ellestad, T. G., Xiu, A., and Angevine, W. M.: Comparison of measured and modeled surface fluxes of heat, moisture and chemical dry deposition, in: Air Pollution Modeling and Its Application XI, edited by: Gryning, S.-E. and Schiermeier, F. A., Plenum Press, New York, 1996.

Ramanathan, V., Crutzen, P. J., Lelieveld, J., Mitra, A. P., Althausen, D., Anderson, J., Andreae, M. O., Cantrell, W., Cass, G. R., Chung, C. E., Clarke, A. D., Coakley, J. A., Collins, W. D., Conant, W. C., Dulac, F., Heintzenberg, J., Heymsfield, A. J., Holben, B., Howell, S., Hudson, J., Jayaraman, A., Kiehl, J. T., Krishnamurti, T. N., Lubin, D., McFarquhar, G., Novakov, T., Ogren, J. A., Podgorny, I. A., Prather, K., Priestley, K., Prospero, J. M., Quinn, P. K., Rajeev, K., Rasch, P., Rupert, S., Sadourny, R., Satheesh, S. K., Shaw, G. E., Sheridan, P., and Valero, F. P. J.: Indian Ocean Experiment: an integrated analysis of the climate forcing and effects of the great Indo-Asian haze, J. Geophys. Res., 106, 28371–28399, 2001.

Ricchiazzi, P., Yang, S., Gautier, C., and Sowle, D.: SBDART: a research and teaching software tool for plane-parallel radiative transfer in the Earth's atmosphere, B. Am. Meteorol. Soc., 79, 2101–2114, 1998.

Roger, J.-C., Mallet, M., Dubuisson, P., Cachier, H., Vermote, E., Dubovik, O., and Despiau, S.: A synergetic approach for estimating the local direct aerosol forcing: applications to an urban zone during the Expérience sur Site pour Contraindre les Modèles de Pollution et de Transport d'Emission (DSCOMPTE) experiment, J. Geophys. Res., 111, D13208, doi:10.1029/2005JD006361, 2006.

Scott, N. A.: A direct method of computation of the transmission function of an inhomogeneous gaseous medium-I: Description of the method, J. Quant. Spectrosc. Ra., 14, 691–704, 1974.

Seinfeld, J. H., Carmichael, G. R., Arimoto, R., Conant, W. C., Brechtel, F. J., Bates, T. S., Cahill, T. A., Clarke, A. D., Doherty, S. J., Flatau, P. J., Huebert, B. J., Kim, J., Markowicz, K. M., Quinn, P. K., Russell, L. M., Russell, P. B., Shimizu, A., Shinozuka, Y., Song, C. H., Youhua, T., Itsushi, U., Vogelmann, A. M., Weber, R. J., Woo, J.-H., and Zhang, X. Y.: ACE-ASIA: regional climate and atmospheric chemical effects of Asian dust and pollution, B. Am. Meteorol. Soc., 85, 367–380, 2004.

ACPD
13, 19193–19235, 2013

Sena, E. T., Artaxo, P., and Correia, A. L.: Spatial variability of the direct radiative forcing of biomass burning aerosols and the effects of land use change in Amazonia, Atmos. Chem. Phys., 13, 1261–1275, doi:10.5194/acp-13-1261-2013, 2013.

Song, C. H., Maxwell-Meier, K., Weber, R. J., Kapustin, V., and Clarke, A.: Dust composition and mixing state inferred from airborne composition measurements during ACE-Asia C130 Flight#6, Atmos. Environ., 39, 359–369, 2005.

Song, C. H., Kim, C. M., Lee, Y. J., Carmichael, G. R., Lee, B. K., and Lee, D. S.: An evaluation of reaction probabilities of sulfate and nitrate precursors onto East Asian dust particles, J. Geophy. Res., 112, D18206, doi:10.1029/2006JD008092, 2007.

Song, C. H., Park, M. E., Lee, K. H., Ahn, H. J., Lee, Y., Kim, J. Y., Han, K. M., Kim, J., Ghim, Y. S., and Kim, Y. J.: An investigation into seasonal and regional aerosol characteristics in East Asia using model-predicted and remotely-sensed aerosol properties, Atmos. Chem. Phys., 8, 6627–6654, doi:10.5194/acp-8-6627-2008, 2008.

Song, C. H., Nam, J. E., Han, K. M., Lee, M. K., Woo, J. H., and Han, J. S.: Influence of mineral dust mixing-state and reaction probabilities on size-resolved sulfate formation in Northeast Asia, Atmos. Environ., 58, 23–34, doi:10.1016/j.atmosenv.2011.10.057, 2012.

Takemura, T., Nakajima, T., Dubovik, O., Holben, B. N., and Kinne, S.: Single-scattering albedo and radiative forcing of various aerosol species with a global three-dimensional model, J. Climate, 15, 333–352, 2002.

US Committee on Extension to the Standard Atmosphere: U.S. Standard Atmosphere, US Government Printing Office, Washington, D.C., 1962.

van Dorland, R., Dentener, F. J., and Lelieveld, J.: Radiative forcing due to tropospheric ozone and sulfate aerosols, J. Geophys. Res., 102, 28079–28100, 1997.

Volkamer, R., Jimenez, J. L., San Martini, F., Dzepina, K., Zhang, Q., Salcedo, D., Molina, L. T., Worsnop, D. R., and Molina, M. J.: Secondary organic aerosol formation from anthropogenic air pollution: rapid and higher than expected, Geophys. Res. Lett., 33, L17811, doi:10.1029/2006GL026899, 2006.

Wang, Z., Akimoto, H., and Uno, I.: Neutralization of soil aerosol and its impact on the distribution of acid rain over East Asia: observations and model results, J. Geophys. Res., 107, 4389, doi:10.1029/2001JD001040, 2002.

Xia, X. and Zong, X.: Shortwave versus longwave direct radiative forcing by Taklimakan dust aerosols, Geophys. Res. Lett., 36, L07803, doi:10.1029/2009GL037237, 2009.

ACPD
13, 19193–19235, 2013

Zhang, H., Wang, Z., Wang, Z., Liu, Q., Gong, S., Zhang, Z., Shen, Z., Lu, P., Wei, X., Che, H., and Li, L.: Simulation of direct radiative forcing of aerosols and their effects on East Asian climate using an interactive AGCM-aerosol coupled system, Clim. Dynam., 38, 1675–1693, 2012.

Zhang, Y., Liu, P., Queen, A., Misenis, C., Pun, B., Seigneur, C., and Wu, S.-Y.: A comprehensive performance evaluation of MM5-CMAQ for the Summer 1999 Southern Oxidants Study episode – Part II: Gas and aerosol predictions, Atmos. Environ., 40, 4839–4855, 2006.

Zheng, J. Y., Yin, S. S., Kang, D. W., Che, W. W., and Zhong, L. J.: Development and uncertainty analysis of a high-resolution NH_3 emissions inventory and its implications with precipitation over the Pearl River Delta region, China, Atmos. Chem. Phys., 12, 7041–7058, doi:10.5194/acp-12-7041-2012, 2012.

Zheng, M., Cass, G. R., Schauer, J. J., and Edgerton, E. S.: Source apportionment of $PM_{2.5}$ in the Southeastern United States using solvent-extractable organic compounds as tracers, Environ. Sci. Technol., 36, 2361–237, 2002.

ACPD
13, 19193–19235, 2013

Table 1. Statistical values between CMAQ-estimated and EANET-derived particulate concentrations of NO_3^-, SO_4^{2-}, and NH_4^+ for 4 seasons, 2006.

Species	Period	Number of data (N)	R [a]	$\overline{\chi^2}$ [b]	RMSE [c]	MNGE [d] (%)	MB [e]	MNB [f] (%)
NO_3^-	Spring	36	0.57	0.98	2.06	145.01	0.96	119.00
	Summer	36	0.33	1.75	0.98	253.05	0.36	203.08
	Fall	35	0.64	20.21	1.12	174.72	0.07	93.91
	Winter	35	0.79	1.54	2.16	448.02	1.15	410.07
SO_4^{2-}	Spring	36	0.56	9.52	4.82	64.60	−3.65	−54.99
	Summer	36	0.51	1.40	2.69	54.72	−1.06	1.19
	Fall	35	0.57	4.42	3.21	53.81	−2.44	−46.61
	Winter	35	0.45	5.63	3.64	44.74	−2.51	−43.31
NH_4^+	Spring	36	0.60	0.49	1.05	54.25	−0.06	26.55
	Summer	36	0.74	0.22	0.68	51.70	0.14	32.73
	Fall	35	0.65	0.35	0.69	46.77	−0.15	2.24
	Winter	35	0.72	0.36	0.93	60.15	0.14	40.33

[a] Regression coefficient, $R = \frac{N\sum_1^N M_i O_i - \sum_1^N M_i \sum_1^N O_i}{\sqrt{N\sum_1^N M_i^2 - \left(\sum_1^N M_i\right)^2}\sqrt{N\sum_1^N O_i^2 - \left(\sum_1^N O_i\right)^2}}$.

[b] Normalized chai square, $\overline{\chi^2} = \frac{1}{N}\sum_i^N\left[\frac{(O_i - M_i)^2}{O_i}\right]$.

[c] Root mean square error, RMSE $= \sqrt{\frac{1}{N}\sum_1^N (M_i - O_i)^2}$.

[d] Mean normalized gross error, MNGE $= \frac{1}{N}\sum_1^N\left(\frac{|M_i - O_i|}{O_i}\right) \times 100$.

[e] Mean bias, MB $= \frac{1}{N}\sum_1^N (M_i - O_i)$.

[f] Mean normalized bias, MNB $= \frac{1}{N}\sum_1^N\left(\frac{M_i - O_i}{O_i}\right) \times 100$ where, M and O indicate CMAQ-estimated and EANET particulate concentrations, respectively.

ACPD
13, 19193–19235, 2013

Table 2. The contribution of ammonium nitrate to AODs and DRFs (Φ_{AOD} [1] and Φ_{DRF} [2]) at AERONET sites and over China (CEC), Korea, Japan, Taiwan, and East Asia under clear-sky and all-sky conditions.

Regions	Symbols	Periods				
East Asia	Φ_{AOD}	0.199 (0.130)	0.072 (0.047)	0.134 (0.134)	0.391 (0.313)	0.199 (0.156)
	Φ_{DRF}	0.196 (0.127)[a] (0.101)[b]	0.072 (0.047)[a] (0.036)[b]	0.134 (0.131)[a] (0.102)[b]	0.389 (0.307)[a] (0.245)[b]	0.198 (0.153)[a] (0.121)[b]
China (CEC)	Φ_{AOD}	0.357 (0.186)	0.113 (0.069)	0.206 (0.198)	0.656 (0.479)	0.333 (0.233)
	Φ_{DRF}	0.348 (0.177)[a] (0.169)[b]	0.109 (0.067)[a] (0.062)[b]	0.202 (0.194)[a] (0.184)[b]	0.651 (0.475)[a] (0.427)[b]	0.328 (0.228)[a] (0.210)[b]
Korea	Φ_{AOD}	0.149 (0.205)	0.084 (0.089)	0.141 (0.138)	0.335 (0.344)	0.177 (0.194)
	Φ_{DRF}	0.149 (0.206)[a] (0.147)[b]	0.086 (0.090)[a] (0.061)[b]	0.145 (0.139)[a] (0.114)[b]	0.343 (0.348)[a] (0.301)[b]	0.181 (0.196)[a] (0.156)[b]
Japan	Φ_{AOD}	0.090 (0.103)	0.020 (0.035)	0.056 (0.081)	0.176 (0.207)	0.086 (0.107)
	Φ_{DRF}	0.091 (0.104)[a] (0.084)[b]	0.021 (0.035)[a] (0.026)[b]	0.056 (0.083)[a] (0.066)[b]	0.179 (0.212)[a] (0.165)[b]	0.087 (0.109)[a] (0.085)[b]
Taiwan	Φ_{AOD}	0.017 (0.053)	0.010 (0.014)	0.018 (0.043)	0.036 (0.105)	0.020 (0.054)
	Φ_{DRF}	0.019 (0.054)[a] (0.049)[b]	0.012 (0.015)[a] (0.011)[b]	0.013 (0.044)[a] (0.026)[b]	0.033 (0.107)[a] (0.039)[b]	0.019 (0.055)[a] (0.031)[b]

[1] $\Phi_{AOD} = \frac{\tau_{w/\_nitrate} - \tau_{w/o\_nitrate}}{\tau_{w/\_nitrate}}$, where $\tau_{w/\_nitrate}$ and $\tau_{w/o\_nitrate}$ indicate AODs including nitrate and excluding nitrate, respectively.

[2] $\Phi_{DRF} = \frac{F_{w/\_nitrate} - F_{w/o\_nitrate}}{F_{w/\_nitrate}}$, where $F_{w/\_nitrate}$ and $F_{w/o\_nitrate}$ indicate DRFs by aerosols including nitrate and excluding nitrate at top of atmosphere, respectively.

[a] Φ_{DRF} was estimated under clear-sky conditions.

[b] Φ_{DRF} was estimated under all-sky conditions.

ACPD
13, 19193–19235, 2013

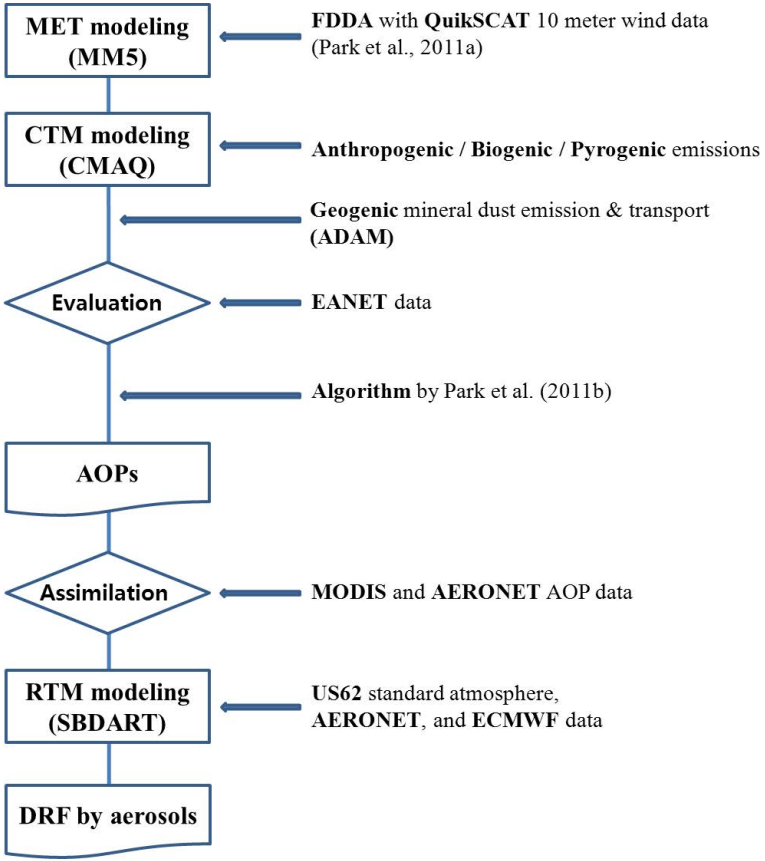

Fig. 1. Flow diagram of the procedures of this study, including: (1) meteorological modeling; (2) US EPA Models-3/CMAQ v4.5.1 modeling; (3) ADAM modeling; (4) assimilations of wind data and aerosol optical properties (AOPs); and (5) SBDART radiative transfer modeling.

ACPD
13, 19193–19235, 2013

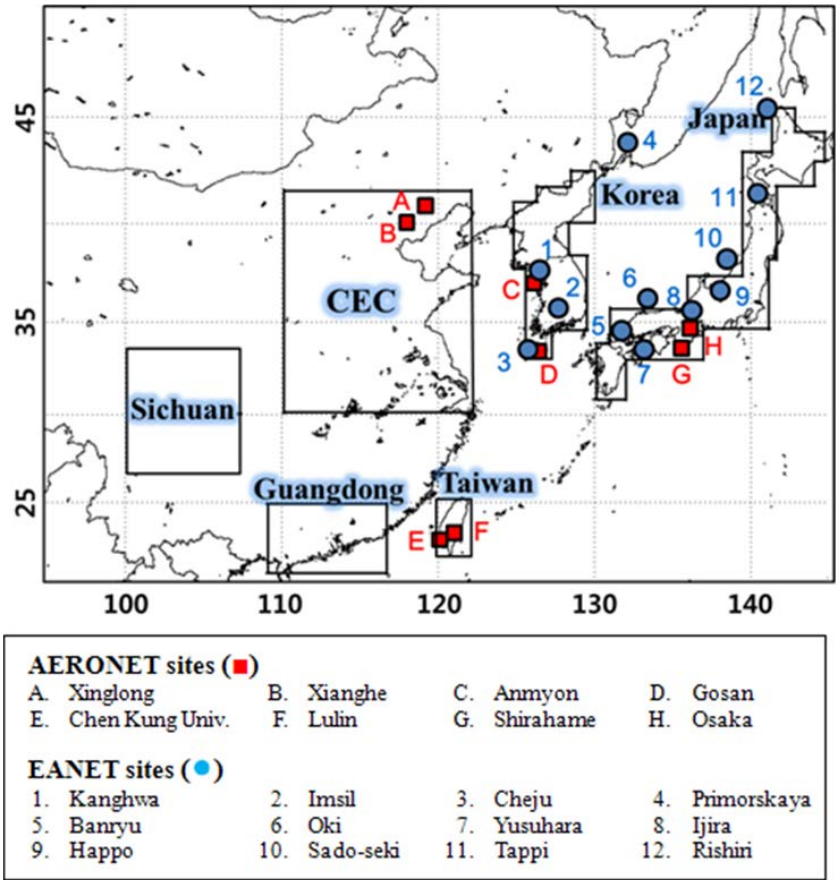

Fig. 2. Model domain of MM5 and CMAQ model simulations and the locations of 8 AERONET sites and 12 EANET sites in the East Asian domain. Also, shown are the Central East China (CEC) region, the Sichuan region, the Guangdong region, Korea, Japan, and Taiwan.

ACPD
13, 19193–19235, 2013

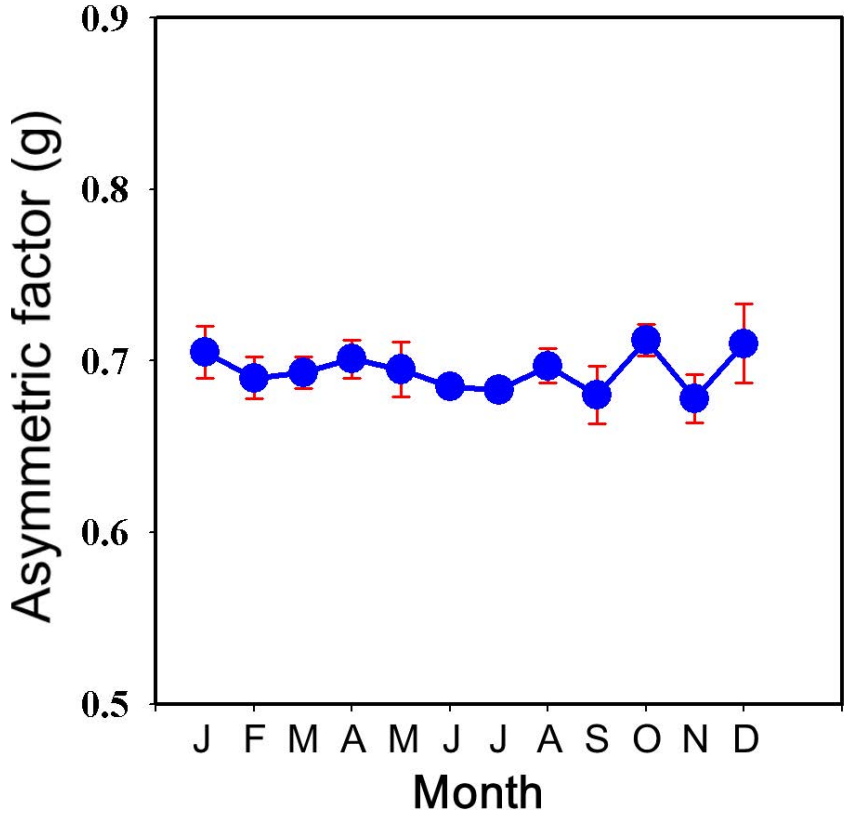

Fig. 3. Mean values of monthly-averaged asymmetric factors (g) from nine AERONET sites for 2006. The red bars indicate $\pm\sigma$ (standard deviation) of the AERONET asymmetric factor.

ACPD
13, 19193–19235, 2013

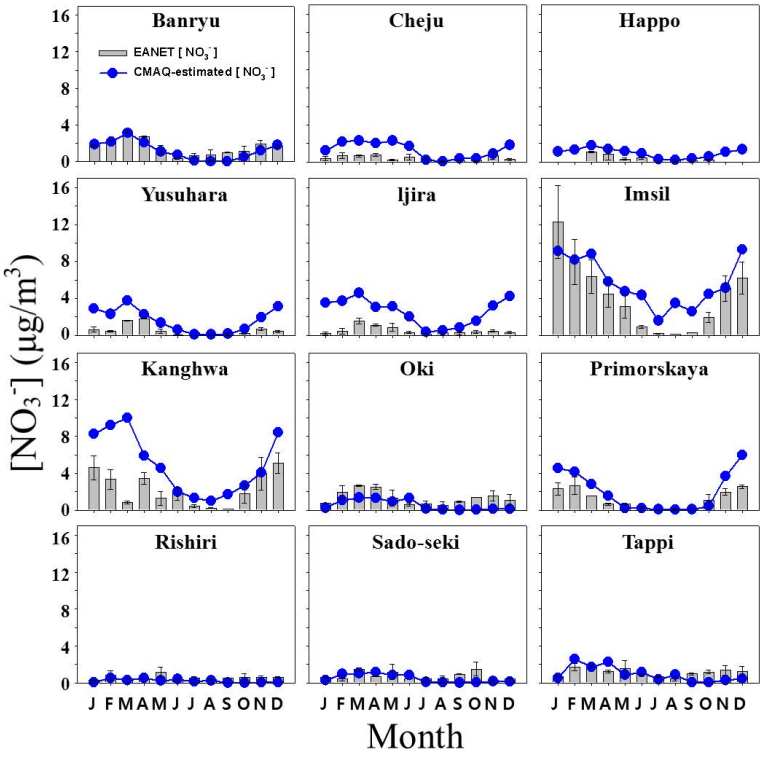

Fig. 4. Comparisons between monthly-averaged EANET concentration of NO_3^- (gray bars) and monthly-averaged CMAQ-estiamated concentration of NO_3^- (blue-dotted lines). The comparisons were made at 12 EANET sites. The black bars indicate the ranges of maxima and minima of EANET NO_3^- concentrations at 9 Japanese EANET sites and $\pm\sigma$ (standard deviation) of EANET NO_3^- concentrations at 3 Korean EANET sites, respectively. Only maxima and minima of daily and biweekly data were obtained from 3 Korean and 9 Japanese EANET sites, respectively. This is because at the 9 Japanese sites only biweekly data were available. In contrast, at the 3 Korean sites the EANET concentrations were based on daily measurements.

ACPD
13, 19193–19235, 2013

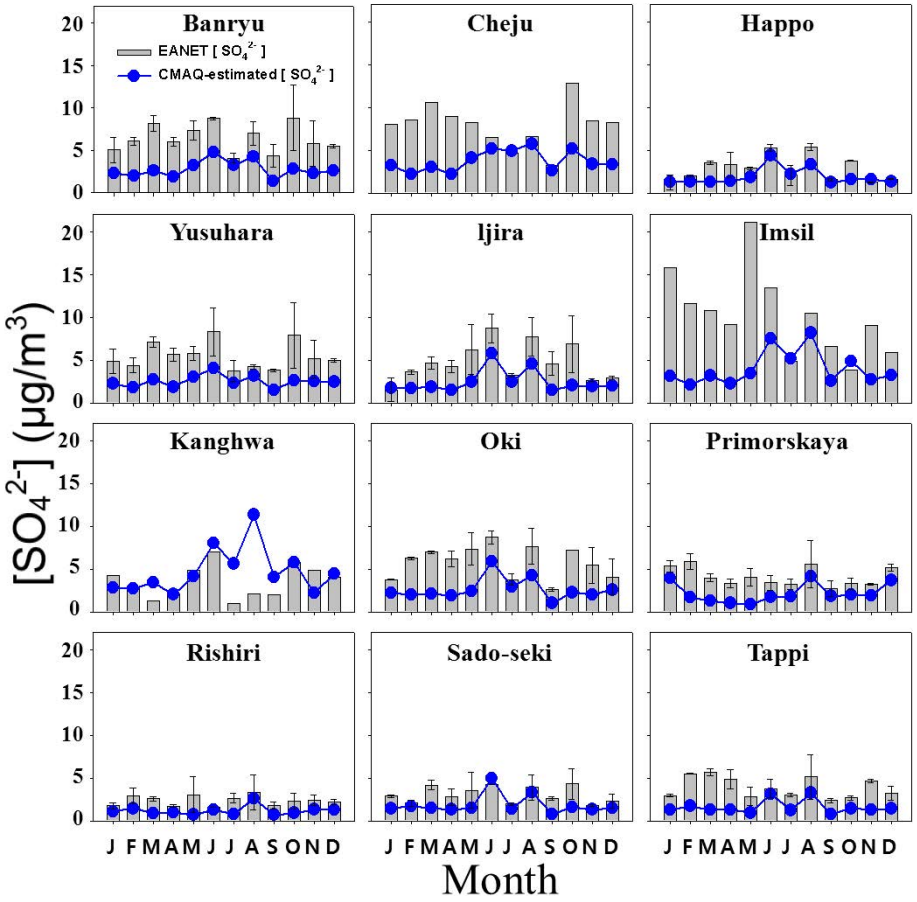

Fig. 5. As Fig. 3, for SO_4^{2-} at 12 EANET sites.

ACPD
13, 19193–19235, 2013

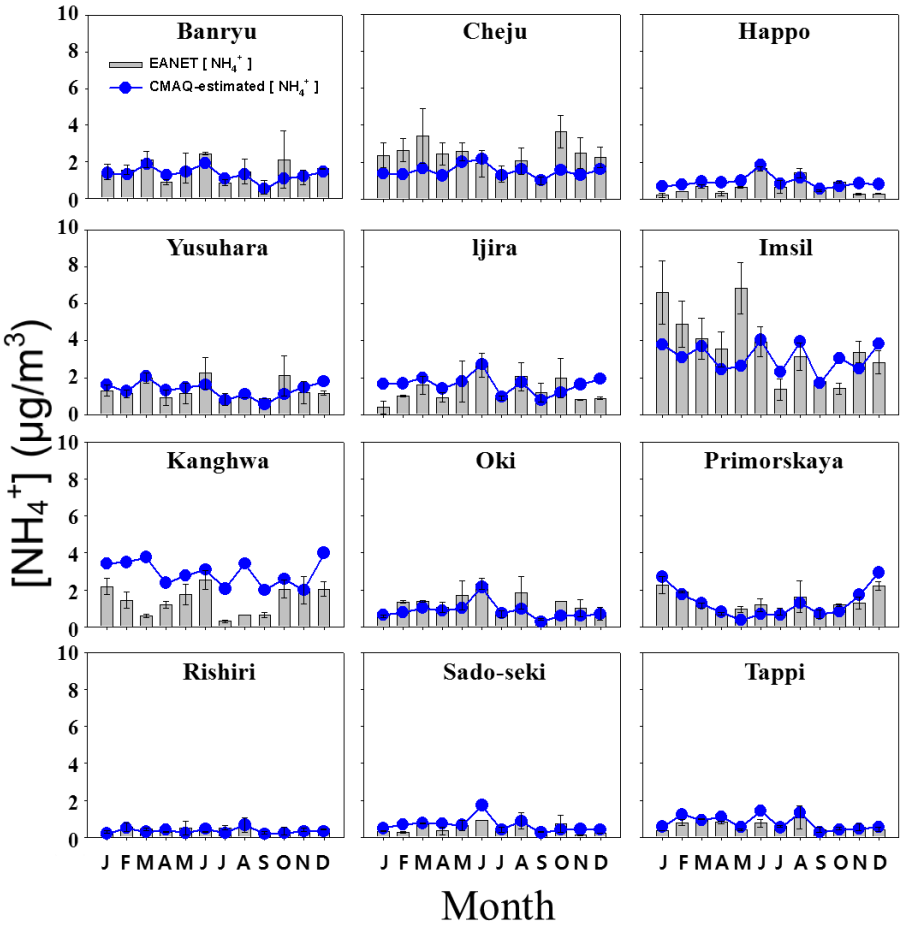

Fig. 6. As Fig. 3, for NH_4^+ at 12 EANET sites.

ACPD
13, 19193–19235, 2013

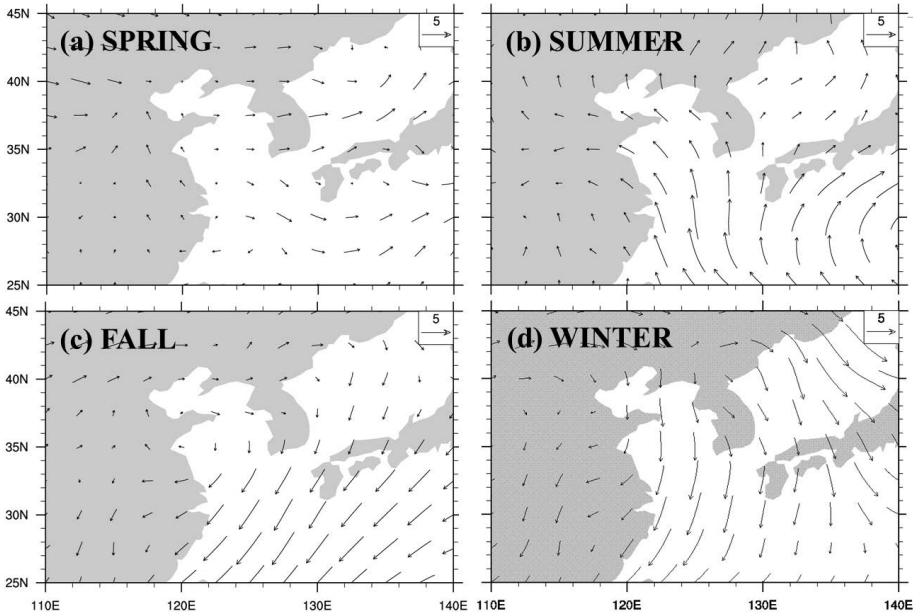

Fig. 7. Seasonally averaged surface wind vectors over East Asia: **(a)** spring, **(b)** summer, **(c)** fall, and **(d)** winter of 2006. The surface wind data was obtained from NCEP/NCAR Reanalysis 1 dataset and the predicted height corresponds to 0.995 of sigma.

ACPD
13, 19193–19235, 2013

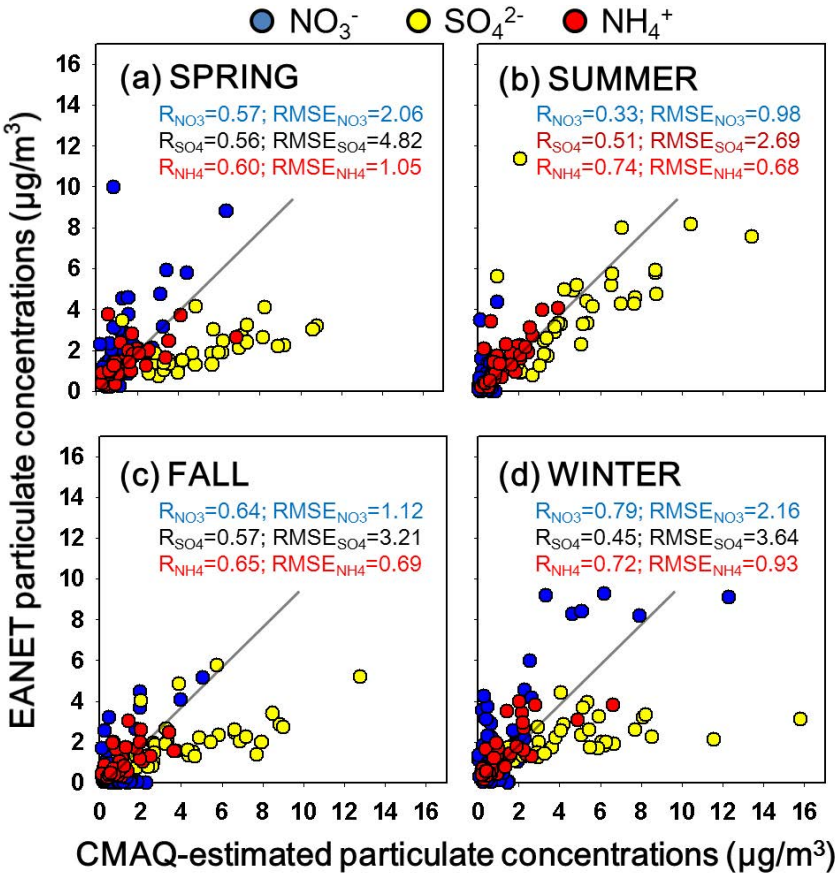

Fig. 8. Scatter plots of CMAQ-estimated and EANET-derived particulate concentrations of NO_3^-, SO_4^{2-}, and NH_4^+ for four seasons, 2006. Blue, yellow, and red circles indicate concentrations of NO_3^-, SO_4^{2-}, and NH_4^+, respectively: **(a)** spring, **(b)** summer, **(c)** fall and **(d)** winter.

ACPD
13, 19193–19235, 2013

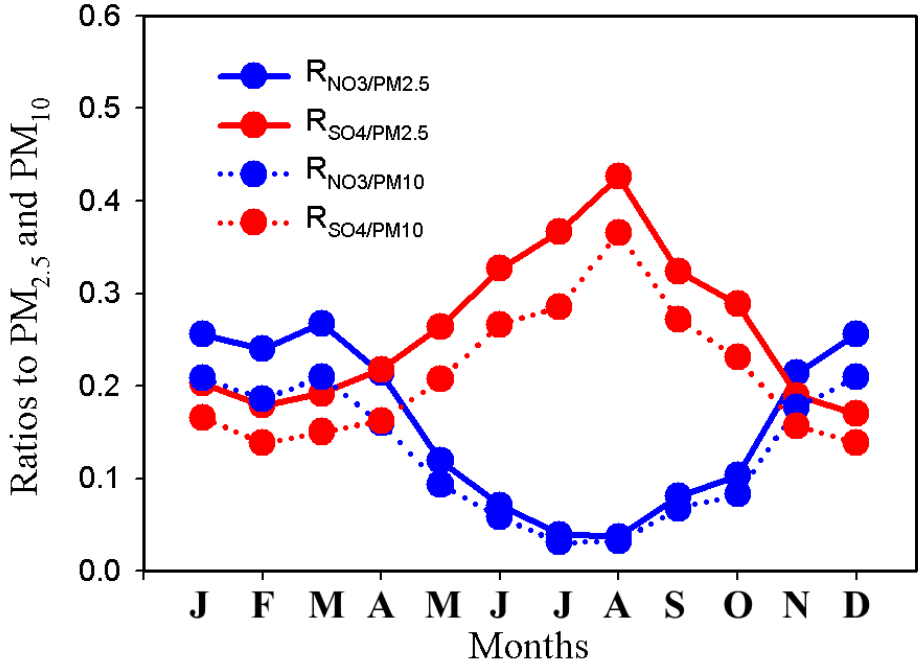

Fig. 9. Monthly-averaged mass ratios of NH_4NO_3 ($R_{NO_3/PM_{2.5}}$ and $R_{NO_3/PM_{10}}$) and $(NH_4)_2SO_4$ ($R_{SO_4/PM_{2.5}}$ and $R_{SO_4/PM_{10}}$) concentrations to $PM_{2.5}$ and PM_{10}.

ACPD
13, 19193–19235, 2013

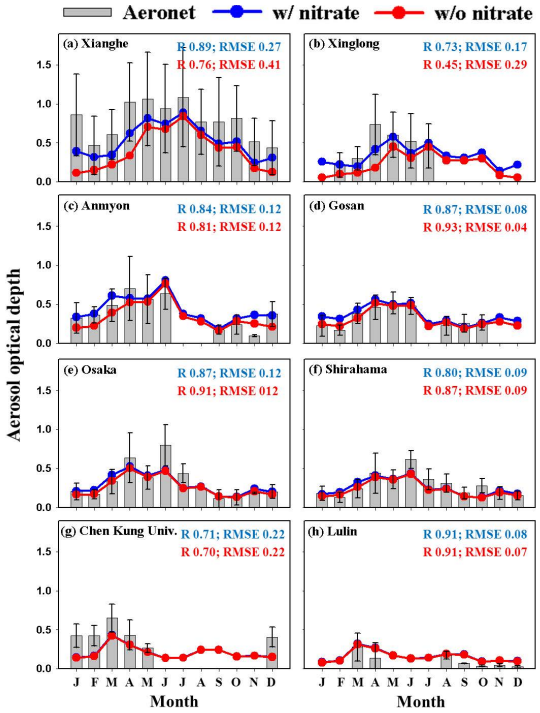

Fig. 10. Comparisons between monthly-averaged AERONET AOD (gray bars) and two monthly-averaged assimilated AODs with and without NH_4NO_3 (blue-dotted and red-dotted lines, respectively). The comparisons were made at 8 AERONET sites. In Fig. 8, R and RMSE represent correlation coefficient and root mean square error, respectively. RMSEs were introduced together with R, because R is very sensitive to the number of data and are not very reliable, in case that the number of data is small. The black bars indicate $\pm\sigma$ (standard deviation) calculated from the daily AERONET AOD data.

ACPD
13, 19193–19235, 2013

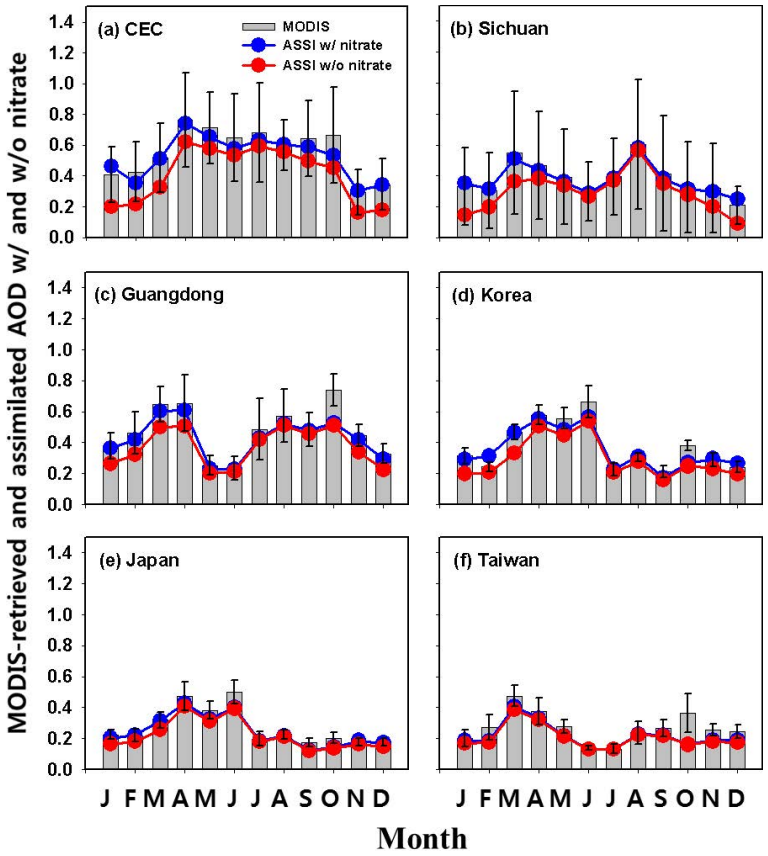

Fig. 11. Comparisons between monthly-averaged MODIS-retrieved AODs (gray bars) and monthly-averaged assimilated AODs *w/* and *w/*o_nitrate (blue-dotted and red-dotted lines, respectively). The comparisons were made at **(a)** Central East China (CEC), **(b)** Sichuan Basin, **(c)** Guangdong, **(d)** Korea, **(e)** Japan, and **(f)** Taiwan. The black bars indicate $\pm\sigma$ (standard deviation) of the spatially-averaged MODIS-retrieved AOD data.

ACPD
13, 19193–19235, 2013

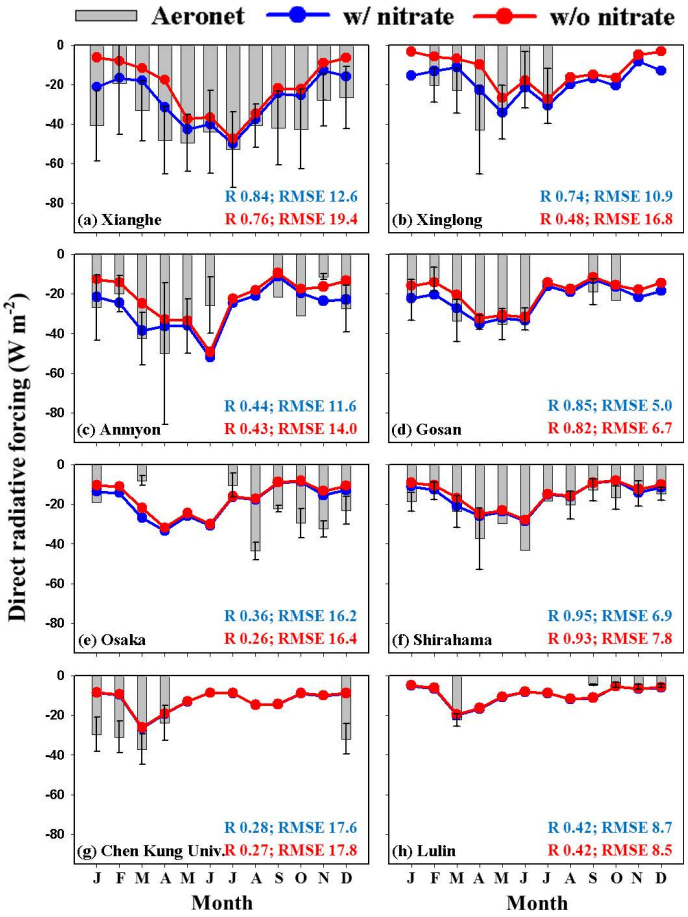

Fig. 12. As Fig. 8, for direct radiative forcing (DRF) by aerosols at 8 AERONET sites. Here, the DRF values (blue- and red-dotted lines) were calculated by SBDART model.

ACPD
13, 19193–19235, 2013

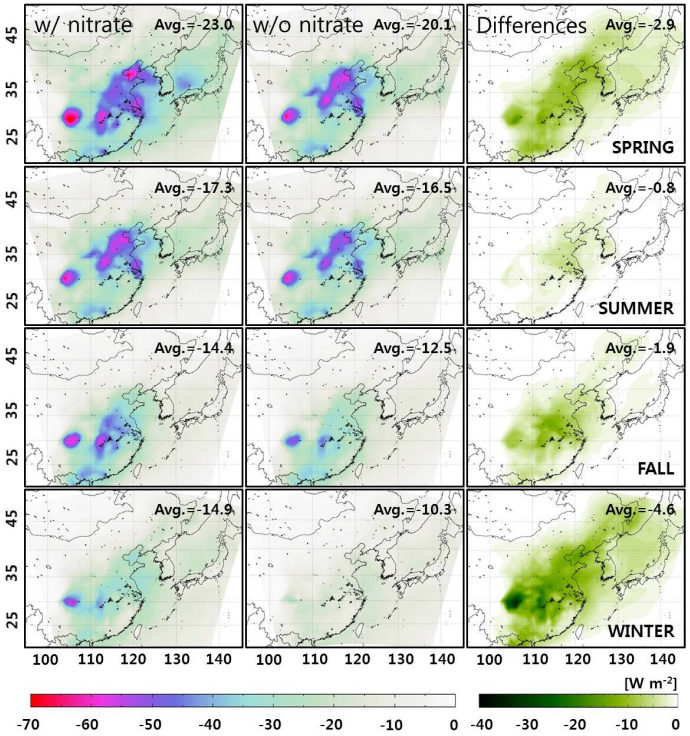

Fig. 13. Direct radiative forcing (DRF) by aerosols under clear-sky conditions estimated by the SBDART simulations for the cases with and without NH_4NO_3 (the first and the second columns) over East Asia for four seasons in 2006. Since the DRF values were calculated with total aerosol composition, they showed large negative values (the first column) in spring and summer. These are due to seasonal formation and/or generation of different particulate species such as ammonium sulfate ($(NH_4)_2SO_4$) and mineral dust. For example, the formation rates of $(NH_4)_2SO_4$ are maximized in summer and are minimized in winter. The third column presents the differences between the first and the second columns. These differences indicate the impacts of NH_4NO_3 on DRF by aerosols in East Asia.

ACPD
13, 19193–19235, 2013

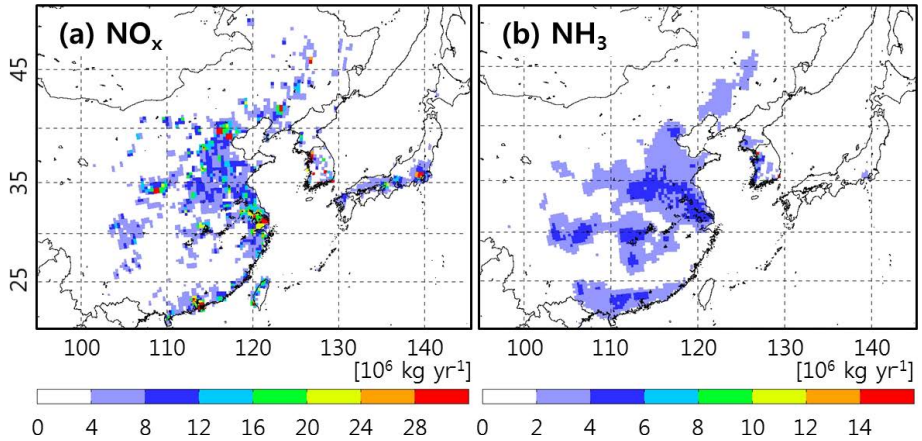

Fig. 14. Spatial distributions of NH_3 and NO_x emissions over East Asia for 2006.

ACPD
13, 19193–19235, 2013

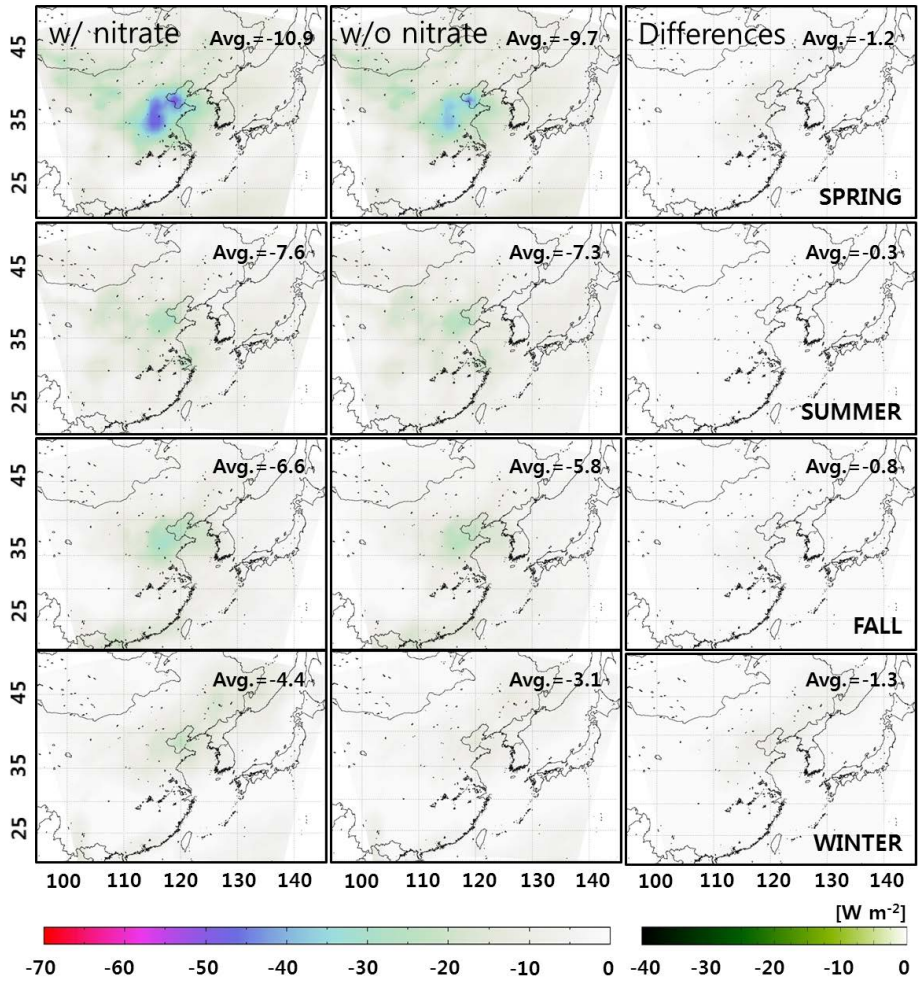

Fig. 15. As Fig. 13, under all-sky conditions.

ACPD
13, 19193–19235, 2013